

## Influence of Surface Reconstruction on the Orientation of Homoepitaxial Silicon Films

R. L. Headrick, B. E. Weir, J. Bevk, B. S. Freer, D. J. Eaglesham, and L. C. Feldman

*AT&T Bell Laboratories, Murray Hill, New Jersey 07974*

(Received 30 April 1990)

Single-crystal silicon films grown at 400°C on Si(111):B( $\sqrt{3}\times\sqrt{3}$ ) are rotated 180° about the surface normal with respect to the substrate. We discuss a mechanism based on chemical effects due to the boron ( $\sqrt{3}\times\sqrt{3}$ ) reconstruction that favors the film to grow with a *B*-type (twin) orientation. Films grown on the Si(111)-(7×7) reconstruction under identical conditions have the *A*-type (untwinned) orientation.

PACS numbers: 68.35.Bs, 61.16.Di, 68.35.Dv

In all prior cases of homoepitaxy, the epilayer has been crystallographically aligned with the substrate, irrespective of the surface reconstruction, impurity segregation, or other effects at the substrate surface. The original surface reconstruction has always reordered into an unreconstructed interface between the substrate and film, since epitaxy requires a sufficiently high temperature for surface diffusion to occur. Here, we describe Si homoepitaxial growth on the boron  $\sqrt{3}\times\sqrt{3}$  surface of Si(111) with  $\frac{1}{3}$  monolayer of boron. At low temperature, the surface reconstruction is partly preserved, buried under an epilayer, and the *homoepitaxial* layer grows rotated by 180° with respect to the substrate. Tung *et al.*<sup>1</sup> have demonstrated rotated *heteroepitaxial* films. We will use their notation; if the substrate orientation is denoted as “*A*-type,” the “*B*-type” orientation corresponds to a layer rotated by 180° about the normal  $\langle 111 \rangle$  direction.

To our knowledge this is the first example of homoepitaxial growth with the overlayer not crystallographically aligned with the substrate. We show experimentally that this phenomenon is critically sensitive to the presence of boron at the original interface during growth, although after growth boron may be in-diffused with no change in film orientation. Modeling suggests that strain effects cannot account for this phenomena. We suggest that the stabilization of the twin boundary interface is related to chemical (electronic) effects which favor a wurtzite stacking at the  $\sqrt{3}\times\sqrt{3}$  interface.

Samples were prepared in a molecular-beam-epitaxy (MBE) chamber equipped with a quartz-crystal thickness monitor, an electron-gun evaporator to deposit silicon, and a Knudsen cell to deposit boron from HBO<sub>2</sub>. Low-energy electron diffraction (LEED) and Auger analysis were performed *in situ*, and x-ray diffraction, transmission electron microscopy (TEM), Rutherford backscattering spectroscopy, nuclear reaction analysis, and Hall-effect measurements were done after removing samples from the MBE chamber. Surfaces were prepared by chemical growth of a thin protective oxide layer before transferring into the vacuum system. The boron  $\sqrt{3}\times\sqrt{3}$  surface reconstruction was prepared either by surface segregation of  $\frac{1}{3}$  monolayer (ML) of boron from boron-implanted samples at 900–1000°C, or

by deposition of boron onto *n*-type samples from HBO<sub>2</sub> while the sample was held at 750°C. The surface structure thus formed is unique to the Si(111)/B system since boron occupies a subsurface site in a fivefold-coordinated substitutional site under a silicon adatom.<sup>2–4</sup> Silicon films of 350 Å were grown on top of the boron  $\sqrt{3}\times\sqrt{3}$  surface reconstruction at temperatures ranging from 350 to 600°C. A comparison of these two different methods of surface preparation showed that *B*-type films were formed on both types of surfaces under the same growth conditions. Several samples, nominally 100% *B*-type films, were furnace annealed at 1000°C for 2 h in a vacuum of  $<10^{-8}$  Torr in order to improve the crystallinity of the film.

Figure 1(a) shows the change of channeling angular widths for the  $\langle 110 \rangle$  and  $\langle 114 \rangle$  directions in films grown at 400°C on  $\sqrt{3}\times\sqrt{3}$  surfaces with initial boron coverage ranging from 0.00 to 0.33 ML. Both directions correspond to an angle of  $\theta=35.26^\circ$  with respect to the surface normal so that a 180° rotation about  $[111]$  interchanges  $\langle 110 \rangle$  and  $\langle 114 \rangle$  directions. By observing the angular width for the film, the orientation of the film relative to the bulk is determined. The  $\langle 110 \rangle$  and  $\langle 114 \rangle$  angular widths at low coverage (0.00–0.11) ML are close to the values measured in bulk crystals, indicating that the orientation of the films is essentially *A* type. The systematically changing angular width at higher coverages shows that the film orientation is a mixture of *A* type and *B* type at 0.22 ML, and is essentially *B* type at 0.33 ML. Figure 1(b) shows a model of the interface and film structure corresponding to 0.0- and 0.33-ML boron coverages on the initial surface.

The influence of the boron reconstruction on the film orientation is also demonstrated in a temperature-dependence study. Figure 2(a) shows the boron Auger signal intensity during Si growth at three different temperatures, indicating the concentration of boron on the surface. When amorphous silicon is deposited at room temperature, the exponentially decreasing boron signal as a function of deposited film thickness is consistent with the escape length of 178-eV Auger electrons from the buried interface; i.e., no significant boron redistribution occurs on a length scale of 5 Å. During growth at higher temperatures, boron segregates along with the growing sur-

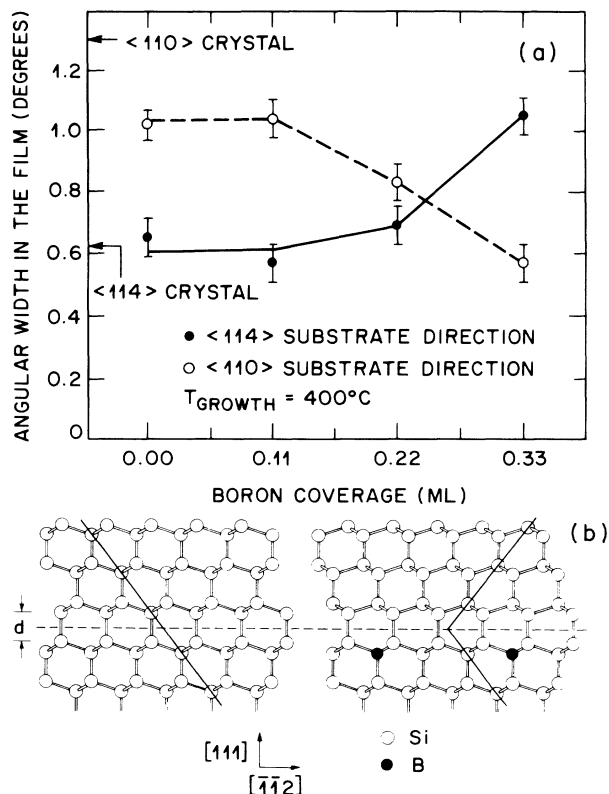


FIG. 1. (a) Angular widths vs boron coverage for (110) and (114) axial channels of the substrate for channeling angular scans with 1.8-MeV  $^4\text{He}^+$  ions with grazing detection at a scattering angle of  $100^\circ$ . The LEED pattern observed on the initial surface was  $7 \times 7$  between 0- and 0.05-ML boron coverage and was  $\sqrt{3} \times \sqrt{3}$  between 0.07- and 0.33-ML boron coverage. The growth temperature and growth rate were  $400^\circ\text{C}$  and  $0.1 \text{ \AA}/\text{sec}$ , respectively. (b) Ball and stick models for the film orientation and interface structure for 0- (left) and 0.33- (right) ML boron coverages. The  $\sqrt{3} \times \sqrt{3}$  reconstruction of the interface is introduced because boron occupies substitutional sites, occupying every third site in a single monolayer at the interface.

face, so that the concentration of boron remaining at the plane of the original surface is reduced. This increased segregation of boron at high growth temperatures is correlated with the film orientation as measured by channeling [Fig. 2(b)]. At  $400^\circ\text{C}$ , where a large fraction of the boron stays at the plane of the original surface, *B*-type films are observed. At temperatures higher than  $540^\circ\text{C}$ , where boron is spread out over a several-hundred-angstrom-thick layer, the films are predominantly *A* type. Table I summarizes the channeling data as a function of boron coverage and temperature.

In addition, grazing-incidence x-ray-diffraction studies of the interface reconstruction were performed. The crystallographic unit cell is chosen so that the in-plane momentum transfer  $q_{\parallel}$  depends on  $h$  and  $k$ , while the perpendicular momentum transfer  $q_{\perp}$  depends only on the index  $l$  (Ref. 5). Rocking scans through  $(\frac{2}{3}, \frac{2}{3})$  near  $l=0$  show that samples with a room-temperature-

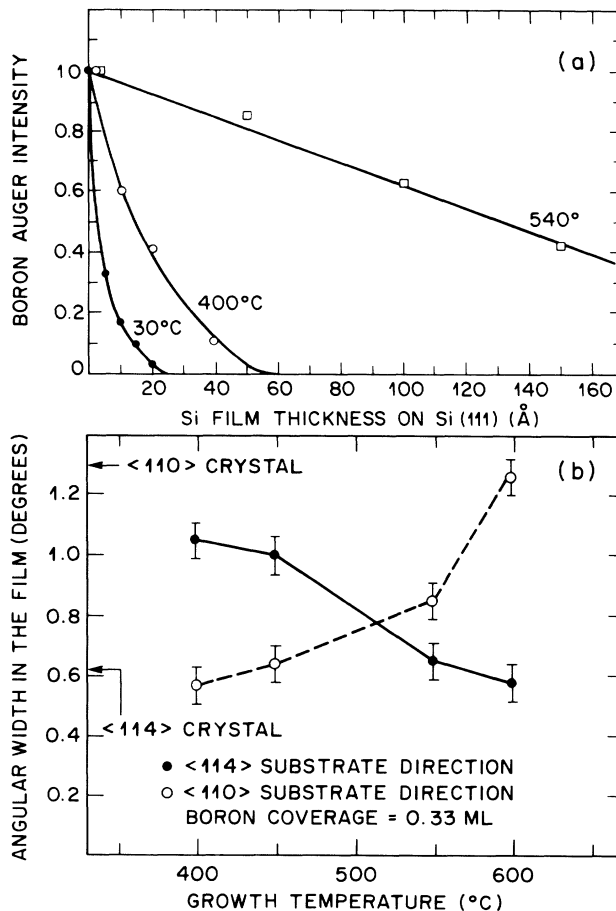


FIG. 2. (a) Intensity of the 178-eV boron Auger transition as a function of silicon film thickness for three different growth temperatures. (b) Angular widths vs growth temperature at 0.33-ML boron coverage for channeling angular scans with 1.8-MeV  $^4\text{He}^+$  ions. The growth rate was  $0.1 \text{ \AA}/\text{sec}$  in both cases.

deposited amorphous silicon cap give a clear signal for the  $\sqrt{3} \times \sqrt{3}$  reconstruction at the interface in agreement with earlier work.<sup>6</sup> In contrast, the  $400^\circ\text{C}$  sample gave a signal with 10% the intensity of the amorphous-capped sample, while the  $540^\circ\text{C}$  sample showed no detectable signal, confirming the disordering of the ordered boron layer with increasing growth temperature.

After annealing *B*-type silicon films at  $1000^\circ\text{C}$  for 2 h, the  $\sqrt{3} \times \sqrt{3}$  interface becomes a simple silicon twin boundary without additional in-plane reconstruction. The presence of boron in the sample can then be ignored because the  $1000^\circ\text{C}$  anneal diffuses boron over an  $\sim 1000 \text{ \AA}$  layer. Below, we characterize the interface structure of an annealed  $350\text{-\AA}$  *B*-type film with x-ray diffraction and transmission electron microscopy.

The x-ray crystal-truncation-rod method using integer  $h$  and  $k$  but continuous  $l$ , originally developed for determination of surface structures, has recently been extended to thin-film structures. A total of 66 data points in the form of structure factors  $F_{hk}(l)$  were obtained by nu-

TABLE I. Summary of the channeling data as a function of boron coverage and temperature.

$T_{\text{growth}}$ (°C)	Minimum yield <sup>a</sup>		Angular width <sup>b</sup> (deg)		Initial boron coverage (ML)
	$\langle 110 \rangle$	$\langle 114 \rangle$	$\langle 110 \rangle$	$\langle 114 \rangle$	
c	0.01	0.04	$1.30 \pm 0.06$	$0.64 \pm 0.06$	...
400	0.02	0.08	1.02	0.65	0
400	0.02	0.08	1.04	0.57	0.11
400	0.59	0.61	0.83	0.69	0.22
400	0.61	0.50	0.57	1.05	0.33
400+1000 anneal	0.25	0.20	0.62	1.05	0.33
450	0.40	0.35	0.64	1.00	0.33
550	0.13	0.16	0.85	0.64	0.33
600	0.01	0.04	1.26	0.58	0.33

<sup>a</sup>Channeling measurements with 1.8-MeV  $^4\text{He}^+$  at room temperature.

<sup>b</sup>The angular width corresponds to the full width at half maximum.

<sup>c</sup>Silicon single crystal with no overlayer.

merical integration of rocking curves and corrected for Lorentz factor ( $\sin 2\theta$ ) and active area ( $\sin \theta$ ). We compared  $(1,0,l)$  crystal-truncation-rod data for a 350-Å *B*-type silicon film grown at 400°C and annealed at 1000°C for 2 h to structure factors calculated in the kinematic approximation.

Figure 3 shows the data for the  $(1,0,l)$  crystal truncation rod. The dashed line is the square of  $F_s(l)$ , the structure factor for the semi-infinite silicon substrate with double-layer termination.<sup>7</sup> The three prominent peaks in the data that do not follow this curve are accounted for by adding the structure factor for a 350-Å-thick *B*-type film,  $F_f(l)$ , into the calculated structure factor as

$$F_{10}(l) = F_s(l) + e^{iq_{\perp}d} F_f(l),$$

where  $d$  is the interface separation and  $q_{\perp} = (2\pi/c)l$ . The agreement of the fit between measured and calculated intensities is evaluated by a standard  $\chi^2$  analysis. The solid line in Fig. 3 shows the results of this calculation with  $N=223$  monolayers and a mixed termination of the top surface of the film (partly double layer and partly single layer). The optimum interface separation was  $d = 2.35 \pm 0.09$  Å, i.e., the same as the bulk layer spacing. This model yielded a  $\chi^2$  of 1.61. Other stacking sequences at the interface that are consistent with a *B*-type film on an *A*-type substrate yield a  $\chi^2 \gtrsim 30$ . This shows that the simple twin stacking sequence is the correct interface structure.

Figure 4 shows a cross-sectional high-resolution TEM micrograph of a 1000°C annealed *B*-type-film/Si(111) sample. A *B*-type film with an atomically sharp interface between the film and substrate is clearly visible. Also, a microtwin defect is visible in the upper right of the figure. A large number of these are present in the film and give rise to the relatively high channeling-

minimum-yield values shown in Table I. These defects are twinned about an off-normal  $\langle 111 \rangle$  direction of the (*B*-type) film.

It is clear from the data described above that the formation of a twin boundary is dependent on preserving the  $\sqrt{3} \times \sqrt{3}$  reconstruction under an epitaxial silicon film and that this is only possible under conditions which kinetically limit the surface segregation of boron. Low-temperature growth is necessary to keep boron trapped

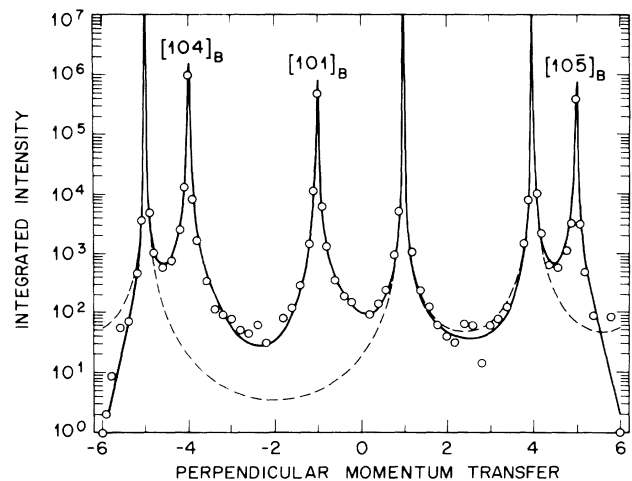


FIG. 3.  $(1,0)$  rod scan for a 350-Å *B*-type Si film on Si(111). A four-circle diffractometer and Cu  $K\alpha$  radiation was used for the measurement. The diffraction profiles are indexed relative to a hexagonal unit cell appropriate for the Si(111) surface with in-plane lattice parameters  $a=b=3.84$  Å and out-of-plane lattice parameter  $c=9.41$  Å. The hexagonal indices are derived from cubic indices by  $[10l]_{\text{hex}} \equiv (1/3)[422]_{\text{cub}} + (l/3)[111]_{\text{cub}}$ . *B*-type reflections are indexed by replacing  $l$  by  $-l$ . Structure factors at  $-l$  were obtained by the symmetry relation  $[10\bar{l}] = [01l]$ .

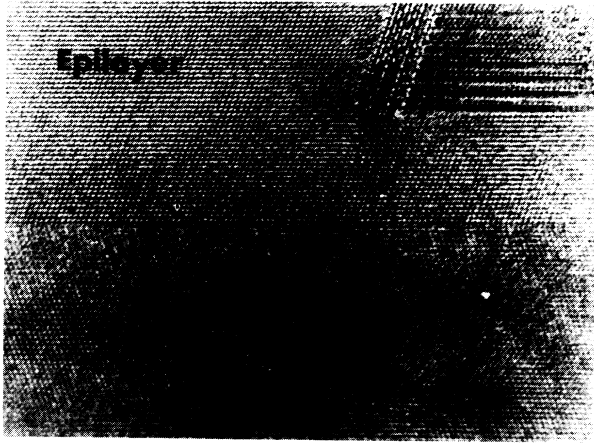


FIG. 4. Cross-sectional high-resolution TEM micrograph of the Si(111)-twin-Si(111) interface. The boron coverage was 0.33 ML and the sample was annealed at 1000°C for 2 h after growth.

at the plane of the original surface, and this surface serves as a template upon which the *B*-type orientation is *energetically preferred*, at least during the nucleation stage of the film growth.

It has been shown previously that the partial monolayer of silicon adatoms that terminate the surface structure become disordered in the presence of excess surface silicon, but that the underlying layers remain ordered.<sup>4</sup> The first epitaxial monolayer then naturally bonds directly to the original surface layer with only a small distortion from perfect tetrahedral bonding due to the presence of boron in a  $\sqrt{3} \times \sqrt{3}$  array. In principle, the strain energy introduced by this distortion could stabilize the *B*-type film relative to the *A*-type film. However, a simple strain-energy model based on bond-angling bending force constants does not predict any difference in the elastic energy between *A*-type and *B*-type films since the magnitude of bond-angle distortions are invariant upon a 180° rotation of the film. Therefore, simple strain-energy considerations do not explain the *B*-type film growth.

Since we cannot rationalize the observation of a *B*-type film through structure arguments, we consider other (chemical) interactions. Silicon prefers the cubic (diamond or zinc blende) stacking sequence over the hexagonal (wurtzite) stacking sequence because the bonding is covalent with no ionic component. A crystal with no ionic character can be thought of as positive cores held together by covalent bonding between nearest neighbors. Wurtzite stacking brings third-nearest neighbors closer than zinc-blende stacking, and so, for silicon, the total energy of the wurtzite structure is larger than that of the diamond structure. In contrast, semiconductors such as the II-VI compounds CdS and ZnO that have a significant ionic component to their bonding prefer the

wurtzite structure, since it is energetically favorable to have (oppositely charged) third-nearest neighbors close together. The site of boron in the  $\sqrt{3}$  reconstruction fills only one of the face-centered-cubic sublattices of the silicon crystal structure, and so the twin boundary formed during overlayer growth can be considered to be a local transformation from zinc-blende to wurtzite stacking.

If the charge transfer between boron and silicon is large enough (as between boron and a surface state<sup>3,4</sup>), then third-nearest-neighbor interactions between boron and silicon would stabilize a stacking fault during the first few layers of film growth [Fig. 1(b)]. In the range of growth temperatures studied, silicon homoepitaxial growth has been found to occur in a two-dimensional island growth and coalescence mode,<sup>8</sup> so that the orientation of the initial island nuclei may determine the orientation of the film after island coalescence. Verification of this model would require a detailed knowledge of the surface structure of the island nuclei and the degree of charge transfer between boron and surface states during the initial stage of the film growth.

In conclusion, boron surface doping of Si(111) is shown to result in a *B*-type homoepitaxial film, when film growth conditions are such that the  $\sqrt{3} \times \sqrt{3}$  reconstruction is preserved at the interface. Such large-area *B*-type homoepitaxial films can be used for fundamentally interesting transport studies associated with electrical transport at boundary interfaces.

We thank A. Ourmazd for use of the JEOL 4000EX electron microscope, R. Pindak and I. Robinson for use of the Rigaku RU-300 x-ray source, and R. Tung for use of one of the molecular-beam-epitaxy chambers. We also thank K. Evans-Lutterodt, A. Levi, F. Unterwald, and W. Savin for valuable contributions.

<sup>1</sup>R. T. Tung, J. M. Gibson, J. C. Beam, J. M. Poate, and D. C. Jacobson, *Appl. Phys. Lett.* **40**, 684 (1982).

<sup>2</sup>R. L. Headrick, I. K. Robinson, E. Vlieg, and L. C. Feldman, *Phys. Rev. Lett.* **63**, 1253 (1989).

<sup>3</sup>P. Bedrossian, R. D. Meade, K. Mortensen, D. M. Chen, J. A. Golovchenko, and D. Vanderbilt, *Phys. Rev. Lett.* **63**, 1257 (1989).

<sup>4</sup>I.-W. Lyo, E. Kaxiras, and Ph. Avouris, *Phys. Rev. Lett.* **63**, 1261 (1989).

<sup>5</sup>I. K. Robinson, W. K. Waskiewicz, R. T. Tung, and J. Bohr, *Phys. Rev. Lett.* **57**, 2714 (1986).

<sup>6</sup>K. Akimoto, J. Mizuki, I. Hirose, T. Tatsumi, H. Hirayama, N. Aizaki, and J. Mizuki, in *Extended Abstracts of the Nineteenth Conference on Solid State Devices and Materials* (Business Center for Academic Societies, Tokyo, 1987); R. L. Headrick, L. C. Feldman, and I. K. Robinson, *Appl. Phys. Lett.* **55**, 442 (1989).

<sup>7</sup>I. K. Robinson, *Phys. Rev. B* **33**, 3830 (1986).

<sup>8</sup>R. T. Tung and F. Schrey, *Phys. Rev. Lett.* **63**, 1277 (1989).

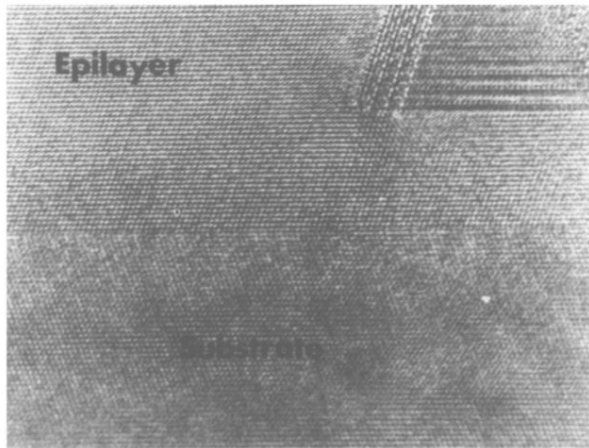


FIG. 4. Cross-sectional high-resolution TEM micrograph of the Si(111)-twin-Si(111) interface. The boron coverage was 0.33 ML and the sample was annealed at 1000 °C for 2 h after growth.